Atmospheric Environment 312 (2023) 120042

Contents lists available at ScienceDirect

Atmospheric Environment

journal homepage: www.elsevier.com/locate/atmosenv

# The impact of COVID-19 lockdowns on urban photochemistry as inferred from TROPOMI

Srijana Lama[a,*], Sander Houweling[a,b], K. Folkert Boersma[c,d], Ilse Aben[b,a], Hugo A.C. Denier van der Gon[e], Maarten C. Krol[c,f]

[a] Vrije Universiteit, Department of Earth Sciences, Amsterdam, the Netherlands
[b] SRON Netherlands Institute for Space Research, Leiden, the Netherlands
[c] Wageningen University, Meteorology and Air Quality Group, Wageningen, the Netherlands
[d] Royal Netherlands Meteorological Institute, R&D Satellite Observations, de Bilt, the Netherlands
[e] TNO, Department of Climate, Air and Sustainability, Princetonlaan, the Netherlands
[f] Institute for Marine and Atmospheric Research Utrecht, Utrecht University, Utrecht, the Netherlands

## HIGHLIGHTS

- The impact of Covid-19 lockdowns on the NOx lifetime is derived using TROPOMI retrieved $NO_2$/CO ratios for six megacities.
- Covid-19 lockdowns reduced the NOx lifetime compared to the year before across the six megacities.
- TROPOMI derived reduction in NOx lifetime over Denver agrees with CLASS model intialized using ground-based observations.

## ARTICLE INFO

*Keywords:*
TROPOMI
Covid-19
$NO_2$
CO
NOx lifetime
Cities

## ABSTRACT

Movement restrictions were imposed in 2020 to mitigate the spread of Covid-19. These lock-down episodes provide a unique opportunity to study the sensitivity of urban photochemistry to temporary emission reductions and test air quality models. This study uses Tropospheric Monitoring Instrument (TROPOMI) nitrogen dioxide/carbon monoxide ($NO_2$/CO) ratios in urban plumes in combination with an exponential fitting procedure to infer changes in the NOx lifetime ($\tau_{NOx}$) during Covid-19 lock-downs in the cities of Denver, Chicago, New York, Riyadh, Wuhan and Sao Paulo compared with the year before.

The strict lockdown policy in Wuhan led to a 65–80% reduction in $NO_2$, compared to 30–50% in the other cities that were studied. In New York and Wuhan, CO concentration was reduced by 10–15%, whereas over Riyadh, Denver, Chicago, and Sao Paulo the CO background concentration increased by 2–5 ppb. $\tau_{NOx}$ has been derived for calm ($0.0 < U$ (m/s) $< 3.5$) and windy ($5.0 < U$ (m/s) $< 8.5$) days to study the influence of wind speed. We find reductions in $\tau_{NOx}$ during Covid-19 lockdowns in all six megacities during calm days. The largest change in $\tau_{NOx}$ during calm days is found for Sao-Paulo (31.8 ± 9.0%), whereas the smallest reduction is observed over Riyadh (22 ± 6.6%). During windy days, reductions in $\tau_{NOx}$ are observed during Covid-19 lock-downs in New York and Chicago. However, over Riyadh $\tau_{NOx}$ is almost similar for windy days during the Covid-19 lockdown and the year before.

Ground-based measurements and the Chemistry Land-surface Atmosphere Soil Slab (CLASS) model have been used to validate the TROPOMI-derived results over Denver. CLASS simulates an enhancement of ozone ($O_3$) by 4 ppb along with reductions in NO (38.7%), $NO_2$ (25.7%) and CO (17.2%) during the Covid-19 lockdown in agreement with the ground-based measurements. In CLASS, decreased $NO_x$ emissions reduce the removal of OH in the $NO_2$ + OH reaction, leading to higher OH concentrations and decreased $\tau_{NOx}$. The reduction in $\tau_{NOx}$ inferred from TROPOMI (28 ± 9.0%) is in agreement with CLASS. These results indicate that TROPOMI derived $NO_2$/CO ratios provide useful information about urban photochemistry and that changes in photochemical lifetimes can successfully be detected.

* Corresponding author. Vrije Universiteit, Department of Earth Sciences, Amsterdam, the Netherlands, De Boelelaan 1085, 1081, HV Amsterdam, Netherlands.
*E-mail addresses:* s.lama@vu.nl, sreejanalama@gmail.com (S. Lama).

https://doi.org/10.1016/j.atmosenv.2023.120042
Received 5 May 2023; Received in revised form 7 August 2023; Accepted 16 August 2023
Available online 18 August 2023

## 1. Introduction

The movement restriction policy implemented by national governments to control the spread of the Covid-19 virus in 2020 had many social, economic and environmental impacts (Bonaccorsi et al., 2020; Chauhan and Singh, 2020; Dhaka et al., 2020; McKibbin and Fernando, 2021). Among the environmental impacts are improvements in air quality, due to reduced emissions of air pollutants associated with the reduced economic activity (Le et al., 2020; Misra et al., 2021). In the past few years, new satellites have been deployed that improve the capacity to monitor air pollution world-wide from space. These measurements offer a great opportunity to investigate the impact of Covid-19 lockdowns on urban air quality. Several studies have demonstrated that trends in urban NOx emissions can be quantified using satellite observations of $NO_2$ (Beirle et al., 2019; Liu et al., 2017; Lorente et al., 2019). Urban CO emissions can be quantified using satellites also, but less accurately than $NO_x$ due to its longer lifetime, complicating the separation of the influence of urban emissions on the observed total column abundances from the background. Nevertheless, a few studies have quantified changes in CO emission from cities using satellite observations (Beirle et al., 2019; Borsdorff et al., 2019; Dekker et al., 2017, 2019; Pommier et al., 2013).

The reduced energy use during Covid-19 lockdowns provides a 'natural experiment' to test the capacity of the existing measurement and modelling infrastructure to monitor the energy transition and its influences on urban air quality. Over central Chinese cities, satellite observations show a decline in tropospheric column $NO_2$ by 30.3%–65.2% (Le et al., 2020). CO mixing ratios decreased by 16.2%–37.9% in ground based measurements (Xu et al., 2020). In the European city of Milan, ground based measurements show a decrease of $NO_2$ by 40%–55% and CO by 25%–30% (Bray et al., 2020; Romano et al., 2021; Vîrghileanu et al., 2020). Similar reductions in $NO_2$ over Milan were detected by Ozone Monitoring Instrument (OMI) observations (Bray et al., 2020). In New York, OMI show reduction in $NO_2$ tropospheric column by 28%–50% and CO concentration decreased by 7%–10% in ground based measurement (Bray et al., 2020). This confirms that reductions in air pollution levels during Covid-19 lockdowns have been measured on ground, but can also be observed from space (Filonchyk et al., 2020; Goldberg et al., 2020; Lange et al., 2021). Miyazaki et al. (2021) studied the change in global photochemistry in response to Covid-19 lockdown and indicate that the free troposphere became less oxidative in response to reductions in NOx emissions. So far, however, changes in the urban photochemical regime and the chemical turn over time of pollutants such as $NO_x$ in urban plume received less attention.

$NO_x$ plays an important role in atmospheric chemistry as it regulates the photochemical production of ozone ($O_3$), for instance in photochemical smog formation, and atmospheric oxidation rates through the recycling of $HO_x$ ($OH + HO_2$). During daytime, the $NO_x$ lifetime ($\tau_{NOx}$) is controlled by the reaction between the hydroxyl radical (OH) and $NO_2$ forming $HNO_3$. The tropospheric OH concentration is strongly influenced by the $NO_x$ concentration due to the non-linear recycling of $HO_x$, causing $\tau_{NOx}$ to be depended on its own concentration (Valin et al., 2013). Additionally, NOx is removed in the formation of dinitrogen penta-oxide ($N_2O_5$), peroxyacetyl nitrate (PAN), and organic nitrates ($RONO_2$).

In the past, OMI $NO_2$ retrievals have been used to determine the NOx emission and lifetime in urban plumes using the exponential modified gaussian (EMG) method by Beirle et al. (2011). The EMG method was modified by Liu et al. (2016) for application to complex emission distributions. The variation of $\tau_{NOx}$ in urban plumes with wind speed has been demonstrated by Valin et al. (2011). The impact of strengthened air pollution mitigation measures in US cities on $\tau_{NOx}$ has been estimated by Laughner and Cohen (2019) using an exponential fitting method applied to OMI $NO_2$ observations. Recently, Lama et al. (2022) presented a method for estimating $\tau_{NOx}$ and the hydroxyl radical in urban plumes, using the regional chemistry transport model WRF in combination with the satellite retrievals of $NO_2$ and CO. This method has the advantage that it can be applied to single satellite overpass. However, the use of an atmospheric transport model is computationally expensive. In this study we adopt a simplified approach using the Tropospheric Monitoring Instrument (TROPOMI) derived $NO_2$/CO ratio to estimate $\tau_{NOx}$ in urban plumes during Covid-19 lockdowns in comparison with other years. On 13 October 2017, the Sentinel-5 Precursor satellite was launched with TROPOMI instrument on board (Veefkind et al., 2012). TROPOMI measures $NO_2$ tropospheric column and CO total column with high sensitivity, high spatial resolution and daily global coverage and is therefore well suited for this task. In this method, CO is used due to its longer lifetime than $NO_2$ and can be considered as inert tracer over the urban area of interest. The difference in the rate of decay between $NO_2$ and CO provides information about the photochemical oxidation of $NO_2$, because atmospheric dispersion is expected to have a very similar impact on both tracers and therefore cancels out in their ratio.

This paper is organized as follows: Section 2 describes the TROPOMI $NO_2$ and CO data that were used, the method used to estimate $\tau_{NOx}$ using TROPOMI derived $NO_2$/CO ratios and the sensitivity tests that are performed to evaluate the robustness of the method. The impact of Covid-19 lockdowns on urban $\tau_{NOx}$ is presented in section 3, followed by its validation using ground based observations and CLASS. The main outcomes of this study are discussed and summarized in sections 4 and 5. Additional figures supporting the result of this study can be found in the supplement.

## 2. Data and method

### 2.1. TROPOMI $NO_2$ tropospheric column

We used the S5P-PAL reprocessed $NO_2$ [mole/m$^2$] data product available at https://data-portal.s5p-pal.com/products/no2.html. In December 2020, the $NO_2$ processor v1.3.2 was upgraded to v1.4.0. The updated FRESCO cloud retrieval in v1.4.0. increased the tropospheric $NO_2$ column by 0%–50% in polluted areas under clear sky conditions (Eskes and Eichmann, 2022; Riess et al., 2022; Van Geffen et al., 2022). In contrast, adjustments in surface albedo in v2.2.0 increased the tropospheric $NO_2$ columns by 10%–15% for polluted cloud free scenes (Eskes and Eichmann, 2022). Therefore, to study the impact of Covid-19 lockdowns on the observed trends in pollutants, $NO_2$ data products v1.2. x and 1.3. x cannot be combined with v1.4.0 and v2.2.0. To restore the consistency of the full dataset, the TROPOMI $NO_2$ data set has been reprocessed for the period from May 1, 2018 to Nov 14, 2021 using the latest operational $NO_2$ processor version 2.3.1.

The TROPOMI $NO_2$ DOAS software developed by KNMI is used to process $NO_2$ slant column densities (van Geffen et al., 2019). The slant column densities are converted into tropospheric column densities using an improved version of the QA4ECV $NO_2$ algorithm (Boersma et al., 2011, 2018). Here, tropospheric slant column densities are obtained by subtracting the stratospheric contribution from slant column densities. Tropospheric slant columns are converted into tropospheric vertical column densities by applying air mass factor (AMF), as function of surface albedo, terrain height, cloud height, cloud fraction and a priori vertical $NO_2$ profile from TM5 model at $1^\circ \times 1^\circ$ resolution (Eskes et al., 2018; Lorente et al., 2017). MAXDOAS ground based measurements over European cities indicate that TROPOMI underestimates tropospheric column $NO_2$ by 7%–29.7% (Lambert et al., 2019). This bias arises from the coarse resolution a priori $NO_2$ profiles used in the AMF calculation.

### 2.2. TROPOMI CO

In this study, offline level 2 CO data version 1.3. x has been used available at https://cophub.copernicus.eu/s5pexp (last access: 20 September 2020). The total CO column [molec cm$^{-2}$] is retrieved from TROPOMI 2.3 μm spectra using the SICOR algorithm (Landgraf et al., 2016). This algorithm uses the profile scaling approach in which TROPOMI-observed spectra are fitted by scaling a reference vertical profile of CO using the Tikhonov regularization technique (Borsdorff et al., 2014). TM5 transport model based reference CO profiles are used in this method (Huijnen et al., 2019; Krol et al., 2005). The sensitivity of TROPOMI-derived total CO columns to the vertical profile of CO is defined by the averaging kernel that is obtained from each retrieval. TROPOMI inferred CO is compared with 28 different Total Carbon Column observing Network (TCCON) measurements, which showed a difference of 9.1 ± 3.3% (Sha et al., 2021).

### 2.3. Satellite data selection and filtering criteria

To study the impact of Covid-19 lockdowns on the urban lifetime of $NO_x$ ($\tau_{NOx}$) six different megacities i.e. Wuhan, Riyadh, Sao Paulo, New York, Denver, and Chicago have been selected. These megacities have been selected to compare $\tau_{NOx}$ under $NO_x$ limited (US cities) and VOC limited regimes (Asian and South American cities: Wuhan, Riyadh and Sao Paulo). Table 1 shows the time periods that have been selected for these six megacities, which vary because the Covid-19 lockdown period differs from country to country. TROPOMI $NO_2$ and CO data selected during the Covid-19 lockdown in 2020 are compared with same period in 2019 to eliminate seasonal influences, except for Wuhan. In Wuhan, the Covid-19 lockdown period started from 23rd Jan to 23rd March 2020 but TROPOMI data from 2nd Feb to 23rd March 2020 and 10th Feb to 23rd March 2019 have been selected to avoid the Chinese new year holiday in both years, and the associated reductions in anthropogenic emission (Gong et al., 2014). Note that hereafter the time period selected in 2020 is referred as "Covid-19" and the 2019 reference period as "pre-Covid-19".

TROPOMI $NO_2$ and CO are derived using different channels in TROPOMI and different retrieval algorithms. Because of this, the $NO_2$ and CO data products have different spatial resolutions and filtering criteria. For data filtering, both algorithms provide a quality assurance value (qa), which ranges from 0 to 1. $NO_2$ retrievals with qa >0.75 have been selected representing clear sky conditions. For CO, retrievals with qa ≥0.70 have been selected indicating clear sky conditions or the presence of low level clouds. The application of the SICOR algorithm to SCIAMACHY data showed that the number of valid observations could be increased by accounting for low level clouds (Borsdorff et al., 2018b, a). The CO data were used after stripe filtering following Borsdorff et al. (2018c). The surface pressure in the CO and $NO_2$ data is used to translate total column CO densities and tropospheric $NO_2$ column densities into dry column mixing ratios of XCO (ppb) and $XNO_2$ (ppb). After data filtering, CO and $NO_2$ data have been co-located by allocating the centre co-ordinate of $NO_2$ retrievals to the CO footprints to account for the difference in spatial resolution between $NO_2$ data (at $3.5 \times 7$ $km^2$) and CO data (at $5.5 \times 7$ $km^2$) as in Lama et al. (2022, 2020).

### 2.4. Separation of calm and windy days

The boundary layer averaged wind speed and wind direction are taken from ECMWF Reanalysis v5 (ERA5) data (retrieved at https://cds.climate.copernicus.eu/cdsapp#!/dataset/reanalysis-era5-pressure-levels?tab=overview, last access: 10th March 2021) at a spatial resolution of 0.25° × 0.25° and 1 hourly temporal resolution. ERA5 wind vectors have been spatially and temporally interpolated to the footprints of the TROPOMI pixels. Days are labelled as calm or windy when the average wind speed within a 50 km radius from the centre of city is in the range of $0 \leq U$ [m/s] $\leq 3.5$ and $5.0 \leq U$ [m/s] $\leq 8.5$, respectively. This segregation is used to study the dependence of the $NO_x$ lifetime on the wind speed as in Valin et al. (2013). There are 6–17 clear sky observation for calm and windy days across the six megacities to quantify the NOx lifetime change during pre-Covid-19 and Covid-19 (see Table S1).

**Table 1**
Cities and time periods selected to study the impact of Covid-19 lockdowns on the $NO_x$ lifetime.

| City | Selected time period in 2019 (Pre-Covid-19) | Selected time period in 2020 (Covid-19) |
|---|---|---|
| Riyadh | 1st April to 10th May | 1st April to 31st May |
| Denver | 1st April to 31st May | 1st April to 31st May |
| New York | 15th March to 31st of May | 15th March to 31st of May |
| Chicago | 26 th March to 31st of May | 26 th March to 31st of May |
| Wuhan | 10th Feb to 23rd March | 2nd Feb to 23rd March |
| Sao Paulo | 24th March to 10th May | 24th March to 10th May |

### 2.5. Method for quantifying the $NO_x$ lifetime

The box rotation method from Lama et al. (2022) has been used to determine the $NO_2$/CO ratio in the urban plume as function of the downwind distance from the city centre. The boxes have a width of 200 km, and lengths of 100 km in upwind direction and 300 km in downwind direction. The box is rotated for every overpass in the direction of the wind using the averaged wind direction at 100 km radius from the centre of city. The rotated box B1 (see Fig. S1) is divided into N rectangular boxes, with lengths ($\Delta x$) of 11 km. The $XNO_2$, XCO and wind speed grid cells that fall within the N rectangular boxes are selected to compute averaged $NO_2$, CO and $NO_2$/CO ratios across the wind for each small boxes. The enhancement of $XNO_2$ and XCO over the background declines at larger distance from the city resulting in inaccurate $\Delta XNO_2/\Delta XCO$ ratios. To avoid this, we use the mean $XNO_2$/XCO ratio instead of enhancement ratios. The travel time [hr] from the city centre for each small box is calculated by dividing the downwind distance by the averaged wind speed for each small box (see Fig. S1).

The decline in the mean of single TROPOMI orbit $XNO_2$/XCO ratios with the travel time is used to determine the lifetime of $NO_x$. An exponential function is fitted to the $XNO_2$/XCO ratios starting from the peak value in the city centre up to 300 km in downwind direction in the form of $y = Ae^{(-x/K)}+c$ (see Fig. 1). Here, A is a fit coefficient quantifying the size of the urban perturbation in the background ratio, x is the travel time, K is $\tau_{NOx}$ and c is the constant background ratio. Note that K represents $\tau_{NOx}$ as the NOx/$NO_2$ ratio presumably does not vary significantly in the downwind direction of the urban plume.

### 2.6. Synthetic performance test

To test the robustness of the method, a sensitivity test has been performed using WRF simulations of $NO_x$ and CO from Lama et al. (2022) for the city of Riyadh. These results were obtained using the passive tracer transport option applied to EDGAR NOx and CO emissions and CAMS-derived OH (for more details see Text S1 and Fig. S2). To determine the $NO_x$ lifetime at mid-day, Lama et al. (2022) computed the first order loss of $NO_x$ from the reaction between $NO_2$ and OH forming $HNO_3$, ignoring other pathways of $NO_x$ loss. In summer, the $NO_x$ lifetime estimated by Lama et al. (2022) was within 10% of full chemistry computations in WRF. The WRF simulated summer (June to July 2018) averaged $NO_2$/CO ratio at the time of TROPOMI overpass for windy days ($5.0 \leq U$ [m/s] $\leq 8.5$) in the urban downwind plume defines test Case 1. In Case 2, emissions of $NO_x$ and CO are reduced 50% and 20%, respectively, but the OH concentration is same as in Case 1. In Case 3, the OH concentration is increased by 40%, whereas NOx and CO emissions are the same as in Case 1. Case 1 is compared with Case 2 and Case 3, to understand the impact of changed emissions and OH concentrations on the estimated $\tau_{NOx}$. The settings of the cases and the resulting $\tau_{NOx}$ estimates derived from WRF and the exponential curve fitting method are listed in Table 2.

Fig. 1 shows WRF simulated $XNO_2$, XCO, $XNO_2$/XCO and the exponential fit to the $XNO_2$/XCO ratio starting from the peak value until 300 km downwind of the city centre for Case 1 to 3. The width of the band of

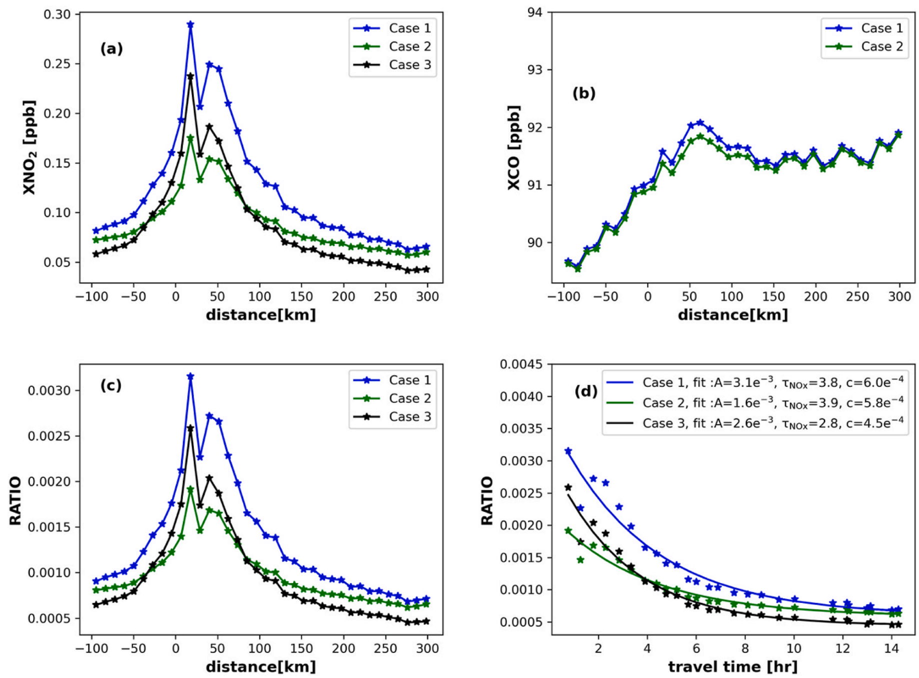


**Fig. 1.** WRF derived a) $XNO_2$, b) XCO, c) $XNO_2$/XCO and d) exponential fit to the $XNO_2$/XCO ratio for Case 1–3. EDGAR $NO_x$ and CO emissions and CAMS OH are input variables for the reference Case 1. In Case 2, $NO_x$ and CO emissions are reduced by 50% and 20% respectively compared to Case 1. In the Case 3, CAMS OH is increased by 40% compared to Case 1. The travel time from the centre of the city is calculated as the ratio of the travel distance and the average wind speed.

**Table 2**
Evaluation of the exponential curve fitting method with WRF simulations for the city of Riyadh.

| Sensitivity test | Description | $\tau_{NOx}$ derived from WRF [hr] (A) | $\tau_{NOx}$ derived from Exponential Fit [hr] (B) |
|---|---|---|---|
| Case 1 | EDGAR NOx and CO emission, CAMS derived OH, NCEP meteorological conditions and CAMS derived NOx and CO boundary condition is used. | 3.7 ± 0.25 | 3.8 ± 0.5 |
| Case 2 | EDGAR NOx emission is reduced by 50% and EDGAR CO emission is reduced by 20%. | 3.7 ± 0.25 | 3.9 ± 0.6 |
| Case 3 | CAMS derived OH is increased by 40%, EDGAR NOx and CO emission as Reference run. | 2.7 ± 0.1 | 2.8 ± 0.3 |

TROPOMI data we consider across the city is wide enough for the diffusing plume to stay within the band. In this case a constant CO enhancement is expected. As discussed in the introduction, Fig. 1 illustrates the exponential decay of $NO_2$ in the downwind urban plume, while CO concentrations remain relatively constant. By calculating the ratio of $NO_2$/CO, valuable insights can be gained regarding the lifetime of NOx. We performed the bootstrapping method for this test to quantify the uncertainty with decreasing data availability on $\tau_{NOx}$. The 1000 samples are generated repetitively by reducing the WRF data size (N) to 50% of the original datasets ($N_R$). Then, $\tau_{NOx}$ is estimated for each of the sample using the exponential curve fitting technique and subsequently, the relative difference between $\tau_{NOx}$ derived for Case 1 compared to other cases is quantified. Using this 1000 samples, the mean and the standard deviation for $\tau_{NOx}$ , and relative difference is derived for Case 1 to 3. For all the tests, $\tau_{NOx}$ derived from WRF and the exponential curve fitting method differs <6% (see Table 2). The $\tau_{NOx}$ derived from an exponential fit to $NO_2$ only is longer by 7.5–10.8% for Case 1 to 3 than using the $NO_2$/CO ratio. This confirms the benefit of applying the exponential curve fitting method to the $NO_2$/CO ratio to estimate $\tau_{NOx}$ in the downwind urban plume. The exponential curve fit successfully recovers the applied OH increase between Case 3 and Case 1 of 40% (37.0 ± 3.7, i.e. within 10%). Overall, the comparison between Case 1 and the other cases confirms that the exponential curve fitting method is sensitive to changes in OH, with sufficient skill in recovering the size of these changes, whereas $\tau_{NOx}$ is insensitive to changes in $NO_x$ and CO emissions (see Table 2).

### 2.7. *Sensitivity test: using TROPOMI data*

Lama et al. (2022) estimated the summer $\tau_{NOx}$ over Riyadh is shorter by 30%–37.5% compared to winter using the EMG and WRF optimization methods. At northern mid-latitudes, the seasonal variation in the incoming solar radiation is larger, increasing the seasonal variation in $\tau_{NOx}$. To test whether our exponential fitting method is capable to resolve variations in $\tau_{NOx}$ using TROPOMI data, it has been applied to TROPOMI derived $NO_2$/CO ratios over Riyadh and Denver in summer (June to August 2019) and winter (November 2019 to January 2020).

Summer and winter averages of TROPOMI retrieved $XNO_2$ and XCO are shown in Fig. 2 and S3 for a domain of 500 × 500 $km^2$ centred around Riyadh and Denver. The $XNO_2$ and XCO enhancements over the background due to city emissions are detected sufficiently well by the satellite to study the seasonal variation in $\tau_{NOx}$. Summer $XNO_2$ is higher by 20%–50% compared to winter $XNO_2$ whereas XCO shows <10% seasonal changes over Riyadh. This is consistent with the use of air conditioning during hot days in Riyadh, increasing the power consumption in summer compared to winter (Lange et al., 2021). The summer and winter averaged $XNO_2$, XCO and $XNO_2$/XCO ratios are derived using the box rotation method for windy days over Riyadh (see Fig. 3). Only windy days could be used for Riyadh in winter, due to insufficient data for calm days. $\tau_{NOx}$ estimates obtained from $XNO_2$/XCO are lower by 7.1% in summer and 16.6% in winter than those obtained using $XNO_2$ only. The exponential fit to $XNO_2$/XCO shows that $\tau_{NOx}$ is shorter in summer compared to winter by 50 ± 14.7% (see Fig. 3d). This means that the seasonal cycle in $\tau_{NOx}$ derived from the exponential curve

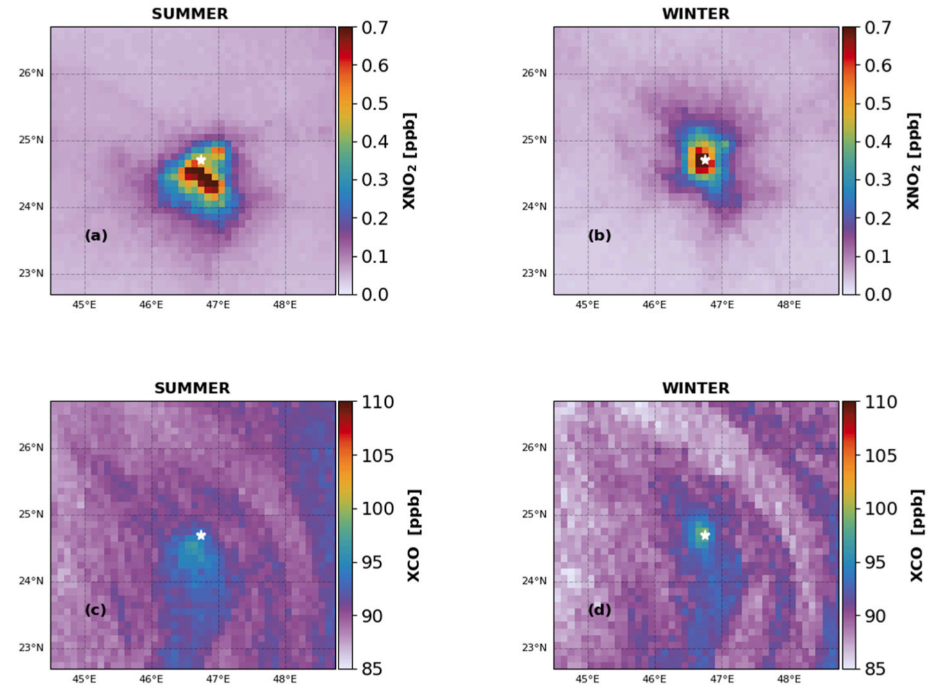


**Fig. 2.** TROPOMI retrieved $XNO_2$ (above) and XCO (below) in summer (June to August 2019) and winter (November 2019 to Jan 2020) over Riyadh. The white star represents the centre of Riyadh.

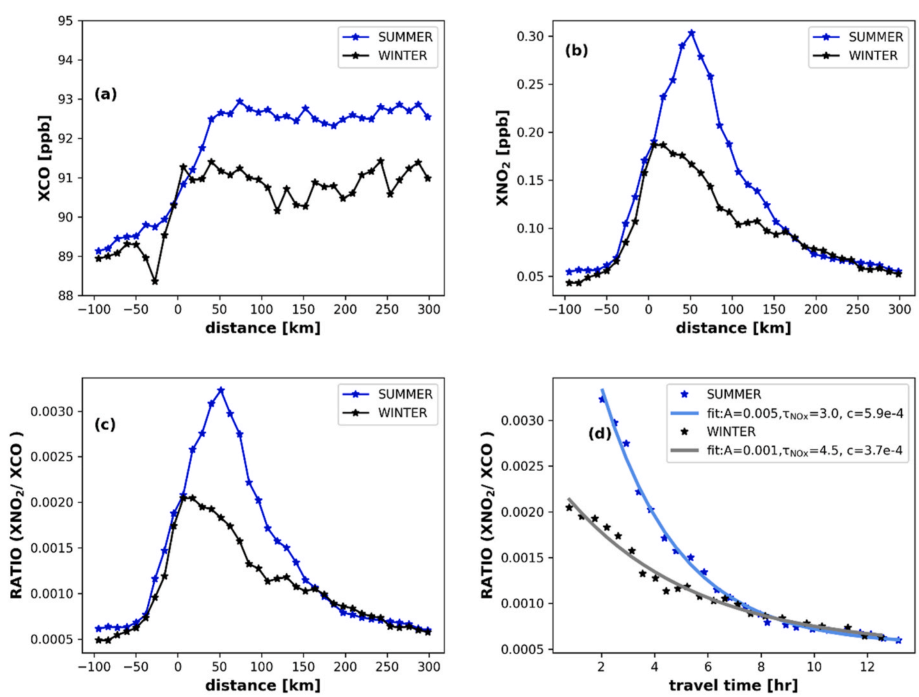


**Fig. 3.** A comparison of summer (June to August) and winter (Nov 2019 to Jan 2020) averages of TROPOMI for windy condition a) XCO, b) $XNO_2$, c) $XNO_2$/XCO, and d) the exponential fit to the XNO2/XCO ratio from the peak value to 300 km downwind distance from Riyadh. The travel time is computed from the ratio of the downwind distance and the averaged wind speed for each box.

fitting applied to TROPOMI $XNO_2$/XCO agrees with Lama et al. (2022). Additionally, boundary layer averaged OH from CAMS over Riyadh at the TROPOMI overpass time is higher by 51.8% in summer compared to winter, in agreement with the seasonal variation in $\tau_{NO_x}$ derived from TROPOMI (see Fig. S4a).

In Denver, summer $XNO_2$ close to the centre of city is smaller by a factor 2.1 to 3.5 compared to winter, whereas the seasonal change in XCO is 6%–12% (see Figs. S3 and S5). During winter, the increased power consumption due to residential heating contributes to higher $XNO_2$ and XCO concentrations compared to summer. The mean $XNO_2$, XCO, and $XNO_2$/XCO ratio are derived for calm days due to insufficient data for windy days. Similar to Riyadh, $\tau_{NO_x}$ derived from $XNO_2$/XCO over Denver is shorter by 17.9% in summer and 14% in winter than using $XNO_2$ only. Fig. S5 shows that for calm days $\tau_{NO_x}$ is shorter by 65.3

$\pm$ 11% in summer compared to winter. This sensitivity test confirms that the exponential curve fitting method applied to TROPOMI derived $XNO_2$/XCO ratios in the downwind urban plume can be used to study the impact of Covid-19 lockdowns on $\tau_{NOx}$. Additionally, CAMS OH is higher by 62% over Denver compared to winter in agreement with TROPOMI (see Fig. S4a).

### 2.8. Boundary layer atmospheric chemistry modelling

In this study, the Chemistry Land-surface Atmosphere Soil Slab (CLASS) model (van Stratum et al., 2012) has been used to support the interpretation of TROPOMI-estimated changes in the urban photochemistry due to the Covid-19 lockdown in Denver. In CLASS the daytime boundary layer growth is determined mostly by the sensible and latent heat fluxes and the entrainment of air from free troposphere. CLASS is a box model for well mixed atmospheric conditions, capable of successfully reproducing the observed mixing ratios of air pollutants and meteorological variables in the turbulent boundary layer (Van Stratum et al., 2012).

CLASS has a simplified Ox-NOx-VOC-HOx photochemistry scheme with 15 reactive species and 28 reactions. CLASS includes night-time chemistry such as the $N_2O_5$ formation and subsequent transformation to $HNO_3$ (Vila-Guerau de Arellano et al., 2009). The simplified chemistry scheme in CLASS incorporates isoprene and its oxidation products but neglects other volatile organic carbon compounds and aerosols (Ouwersloot et al., 2012). Nevertheless, CLASS is able to simulate the observed diurnal cycle and concentrations of important reactants in the polluted atmosphere, as has been shown such for the Amazon and Paris (Lorente et al., 2019; Van Stratum et al., 2012; Vila-Guerau de Arellano and Pino, 2009). CLASS has the advantage over other models that it is computationally cheap, but still includes diurnal changes in the boundary layer and can be used to interpret the various observations (Lorente et al., 2019; Zara et al., 2021).

CLASS has the advantage over 3D chemistry transport models that the settings can be adjusted relatively easily to reproduce observed air pollutants. The CLASS simulation starts at 8 LT (sunrise) with initial conditions for NO, $NO_2$, CO and $O_3$ constrained from ground based observations over Denver (see section 3.4 for details). Additionally, an initial boundary layer height at 8 LT is taken from ERA5 over Denver. The soil moisture is setup such that CLASS simulates a 2000 m boundary layer height at 13–14 LT as in ERA5. In our idealized CLASS simulation for clear sky conditions (without meteorological differences between pre-Covid-19 and Covid-19 lockdown), NOx, CO, isoprene emissions and the dry deposition velocity of $O_3$ are adjusted to reproduce the observed diurnal variability of NO, $NO_2$, CO, and $O_3$ mixing ratios.

## 3. Results

### 3.1. $XNO_2$ and XCO changes during Covid-19

To study an impact of Covid-19 lockdowns on urban photochemistry, TROPOMI data within a domain of 500 $\times$ 500 $km^2$ over Riyadh are averaged from 1st April to 31st May 2020 and for the same period in 2019 (see Fig. 4). TROPOMI-derived $XNO_2$ and XCO enhancements are separated clearly from the background concentration values. During pre-Covid-19 and Covid-19, the longer CO lifetime explains why the CO plumes extend further in the south eastward direction than the corresponding $NO_2$ plumes. During the Covid-19 lockdown $XNO_2$ is reduced by 20%–40% over Riyadh compared with the previous year. In contrast, the XCO background is increased by 3 ppb–5 ppb during Covid-19 compared to pre-Covid-19.

TROPOMI data from April to May 2019 and 2020 are averaged over Denver to analyse the effect of the Covid-19 lockdown (see Fig. S6). During this period, the wind is mostly southerly. TROPOMI retrieved $XNO_2$ reduces by 40–50% due to the lockdown compared with the same period a year earlier. Like Riyadh, the background is higher by 2–6 ppb than during Covid-19. In the other analyzed cities Chicago, New York, and Sao-Paulo, $XNO_2$ is reduced by 30–50%, whereas $XNO_2$ is more strongly reduced Wuhan (65–80%) due to the more strict home stay order during the Covid-19 lockdown (see Figs. S7–S10). In New York, Sao Paulo and Wuhan, XCO close to city centre is reduced by 10–12% during Covid-19 lockdowns. For Chicago, XCO in the urban plume is higher by 5–7%, while the background XCO is higher by 2–5 ppb like in Denver and Riyadh (Fig. S8). The CO background has increased in a few cities due to the influence of regional biomass burning, however, with a

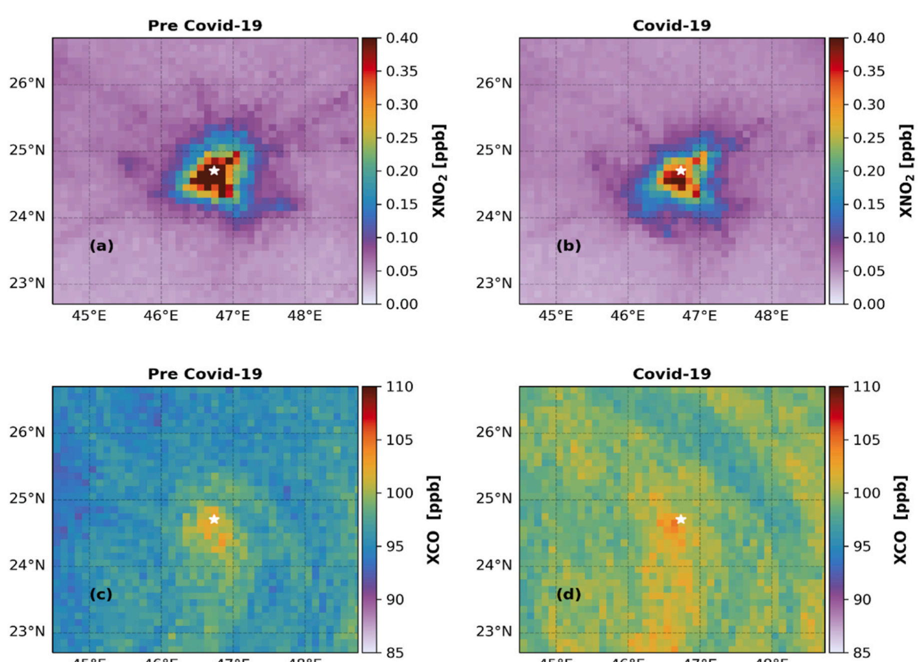


**Fig. 4.** TROPOMI retrieved $XNO_2$ (above) and XCO (below) for pre-Covid-19 (1st April to 31st May 2019) and Covid-19 (1st April to 31st May 2020) over Riyadh. The white star represents the centre of Riyadh.

limited influence on the urban photochemistry. A recent study by Miyazaki et al. (2021) showed that the free troposphere has become less oxidative in response to NOx emission reductions resulting in a decrease in OH at large scales. This could also explain the increase in background CO.

### 3.2. $NO_x$ lifetime ($\tau_{NOx}$) in urban plume during pre-covid-19 Vs Covid-19

Using the box rotation method, daily averaged $XNO_2$, XCO and $XNO_2$/XCO ratios have been derived for Riyadh for calm (see Fig. 5) and windy days (see Fig. S11) during pre-Covid-19 and Covid-19. During calm days, the peak $XNO_2$/XCO ratio is close to the centre of the city. The $XNO_2$/XCO ratio decays most rapidly at intermediate downwind distance (30 km < x < 60 km). At further downwind distance $XNO_2$/XCO decays again more slowly, due to the combined effect of spatial variation of emission sources and diverse NOx removal pattern within the downwind urban plume (see Fig. 5c). On calm days during Covid-19, the $XNO_2$/XCO ratio close to the city centre is reduced by 20–30%, explained mostly by $XNO_2$. On calm days over Riyadh during Covid-19, $\tau_{NOx}$ is 3.9 h, which is shorter by 22 ± 6.6% than during pre-Covid-19 (see Fig. 5 d). $\tau_{NOx}$ has been derived for the six megacities by fitting an exponential function to TROPOMI derived $XNO_2$/XCO ratios in the downwind urban plume during calm and windy days (see Fig. 6 and Fig. S11 to Fig. S17). $XNO_2$/XCO for data during windy days were available days could only be derived for Riyadh, New York, and Chicago because of insufficient windy data were available for the other cities. The uncertainty in $\tau_{NOx}$ for the six cities has been quantified by adding the contributions of the fitted parameters (A, $\tau_{NOx}$ and C), wind speed, width, length of the box and the background in quadrature (see Tables S2 and S3 and Text S2). The total uncertainty for TROPOMI derived $\tau_{NOx}$ ranges from 10 to 20% across the six megacities.

Over Denver, $\tau_{NOx}$ for calm days is shorter by 28 ± 9% during Covid-19 than pre- Covid-19, explained mostly by reductions in $XNO_2$ (Table S4). In other US cities, i.e. Chicago, we also observe shorter $\tau_{NOx}$ during Covid-19 lockdowns. Over Wuhan, Covid -19 $\tau_{NOx}$ derived by fitting $XNO_2$/XCO ratio is 4.7 ± 0.7 h which differs <15% from Zhang et al. (2023). This difference is within the uncertainty range and confirms that the exponential curve fitting method yields realistic estimates of $\tau_{NOx}$ in the urban plume. The more strict home order policy over Wuhan results in stronger reductions in $NO_2$ (65–80%) but $\tau_{NOx}$ is only reduced by 24.2 ± 5% during Covid-19. The largest difference in $\tau_{NOx}$ during pre-Covid-19 and Covid-19 is observed during calm days over Sao-Paulo (31.8 ± 9%) whereas the change in $\tau_{NOx}$ is relatively small over Riyadh compared to other cities (see Fig. 6, S17 and Table S4). Overall, reductions in $\tau_{NOx}$ are found for all the six megacities during Covid-19 lockdowns during calm days (see Fig. 6 and Table S4). On windy days $\tau_{NOx}$ is reduced also during Covid-19 in New York and Chicago, consistent with the calm days. On windy days over Riyadh, however, $\tau_{NOx}$ is almost similar during Covid-19 and pre-Covid-19 (see Fig. S11d).

The $\tau_{NOx}$ for calm and windy days is compared to determine the impact of wind on the $NO_x$ removal in urban plumes. On windy days over Riyadh, the peak in the $XNO_2$/XCO ratio is shifted 30 km away from

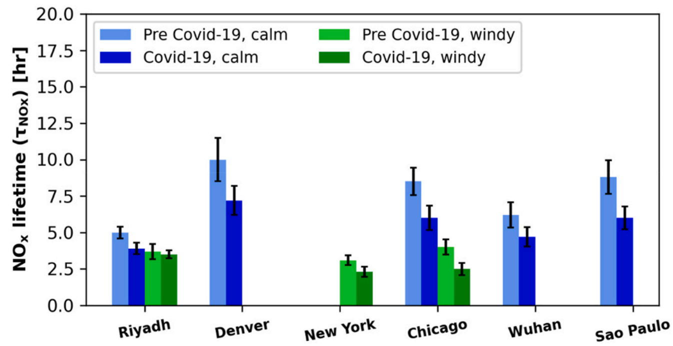


**Fig. 6.** Comparison of $NO_x$ lifetimes derived using the exponential fitting method applied to TROPOMI derived $XNO_2$/XCO ratios in downwind urban plumes during pre- Covid-19 and Covid-19 for calm condition (shades of blue) and windy conditions (shades of green). Light shades are for pre- Covid-19 and dark shades for Covid-19. Error bars represent the uncertainty in $\tau_{NOx}$ derived by adding the contributions from wind speed, fitted parameters, width, length of the box and background correction in quadrature.

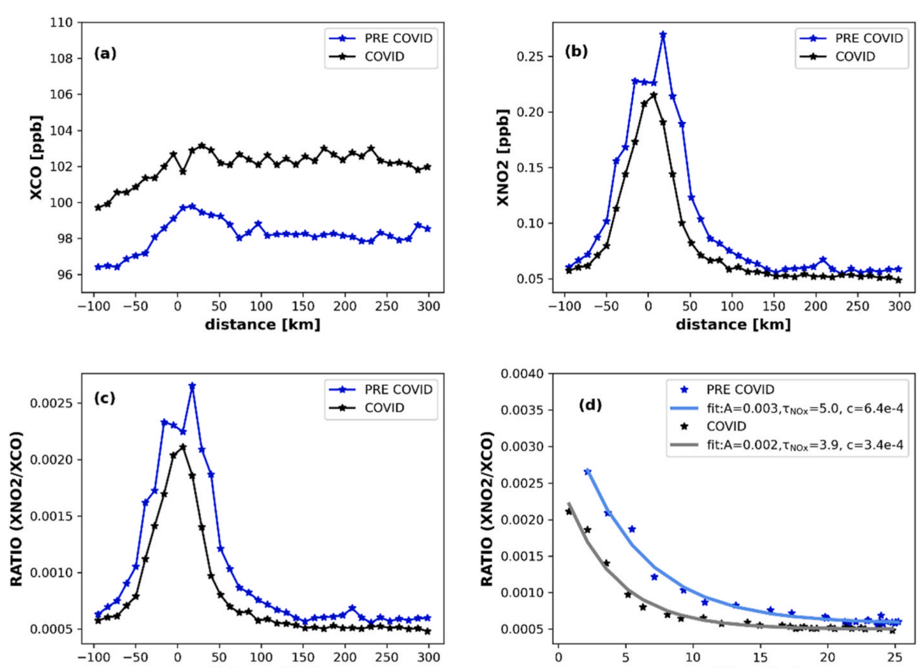


**Fig. 5.** Pre-Covid-19 (1st April to 31st May 2019) vs Covid-19 (1st April to 31st May 2020) TROPOMI averaged across the wind direction for each small boxes for calm conditions a) XCO, b) $XNO_2$ c) $XNO_2$/XCO and d) the exponential fitting of the $XNO_2$/XCO from the peak point to the downwind distance over Riyadh. The travel time is derived by taking the ratio of travel distance by the average windspeed for each of the small boxes.

the centre of city and is lower by a factor 1.6 compared to calm days, which can be explained by the difference in atmospheric advection and mixing (see Fig. 5 and Fig. S11). As expected, on windy days the $NO_2$ and CO plume extend >200 km in the downwind direction (see Fig. S11). This demonstrates how TROPOMI can detect the impact of atmospheric transport on the shape of $NO_2$ and CO plumes. Over Riyadh, $\tau_{NOx}$ is shorter on windy days than on calm days pointing to differences in the $NO_x$ removal, which is expected to be slower during strong pollution episodes. On windy days, the plume is dispersed more quickly leading to lower NOx concentrations. Lower, but still enhanced $NO_x$ leads to more $O_3$ and, in turn, higher OH in the plume of a strong emission source (Vinken et al., 2011). On calm days, pollution accumulates increasing $\tau_{NOx}$, as discussed in the supplement of Lorente et al. (2019). The differences in $\tau_{NOx}$ between calm and windy days are higher during pre-Covid-19 (26.0%) than during Covid-19 (12.5%). Over Chicago, shorter $\tau_{NOx}$ is found during the windy days consistent with Riyadh. The difference in $\tau_{NOx}$ between calm and windy conditions is a factor 2 to 2.5 larger for Chicago than Riyadh. The ERA5 boundary layer over Chicago is shallower during calm days (1106 m) compared to windy days (1737.2 m) by a factor 1.6. The reduced vertical and horizontal mixing during calm days, supressing OH in reaction with $NO_2$ can explain the longer $\tau_{NOx}$ (Lorente et al., 2019). This demonstrates that TROPOMI derived $XNO_2$/XCO can be used to study the functional dependence of the $NO_x$ lifetime on wind speed as mentioned by Valin et al. (2013).

### 3.3. Comparison between TROPOMI derived $\tau_{NOx}$ and CAMS derived OH

TROPOMI derived $\tau_{NOx}$ during calm and windy conditions has been compared to CAMS derived OH. NOx and CO emission reductions during the Covid-19 lockdown are not accounted for in CAMS, except over Europe. Therefore, with limit the comparison between TROPOMI derived $\tau_{NOx}$ and CAMS OH to the pre-Covid-19 period. During calm days, boundary layer averaged OH in CAMS is highest over Riyadh (465 ppq) and lowest over Sao Paulo (290 ppq) among the six selected megacities (see Fig. S4). TROPOMI-derived $\tau_{NOx}$ is shortest for Riyadh (5.0 h), consistent with CAMS. Comparing Sao Paulo to Riyadh, CAMS OH is lower by 43% in excellent agreement with TROPOMI derived $\tau_{NOx}$ being longer by 38%. A similar agreement is found between CAMS OH and TROPOMI-derived $\tau_{NOx}$ over Chicago. Over Denver, however, CAMS OH is 398.5 ppq, which is smaller by 15% compared to Riyadh, whereas TROPOMI shows the longest $\tau_{NOx}$ (10 h) among the selected six megacities. Over Wuhan we also find a disagreement between CAMS OH and TROPOMI-derived $\tau_{NOx}$, where TROPOMI shows a shorter $\tau_{NOx}$ during windy days than during calm days in contrast to CAMS OH (see Fig. S4). This might be explained by the resolution of the CAMS model being to coarse (40 km × 40 km) to resolve the urban accumulation of air pollutants.

### 3.4. Validation using ground-based measurements

To better understand the impact of Covid-19 lockdowns on the photochemical regime in urban plumes and $\tau_{NOx}$, ground-based measurements from Denver have been analyzed (https://aqs.epa.gov/aqsweb/airdata/download_files.html, accessed on 10th Jan 2022) for the period of April to May in 2019 and 2020. Denver has nine ground-based measurement stations for ozone ($O_3$) and six stations for $NO_2$ and NO measurements. For CO, data from four ground-based measurement stations are available (see Fig. S18 for a map of measurement stations).

The hourly data are spatially averaged to obtain average diurnal cycles of $O_3$, $NO_2$, NO, and CO during Covid-19 and pre- Covid-19 (see Fig. 7). In Denver, NO and $NO_2$ concentrations were reduced by 38.7% and 25.7%, respectively, during the Covid-19 lockdown. This means that the satellite measurements show a larger $NO_2$ reduction (40–55%) compared to the ground-based measurements. During the Covid-19 lockdown, CO mixing ratios decreased by 17.2%. The $O_3$ concentration increased by 4 ppb at the time of TROPOMI overpass compared to pre- Covid-19. To analyse the impact of the Covid-19 lockdown in Denver in further detail, we divide the lockdown period into two parts: a) The beginning of the Covid-19 lockdown in the month of April and b) at the midst of Covid-19 lockdown in the month of May. In the beginning of the Covid-19 lockdown, mid-day NO and $NO_2$ decreased by ~28.2% and $O_3$ increased by 2.4 ppb (see Fig. S19). However in May, NO shows a larger reduction (54.8%) compared to April at the time of TROPOMI overpass (see Fig. S20). NOx and volatile organic compounds (VOCs) are the main precursors of photochemical $O_3$ production in the PBL.

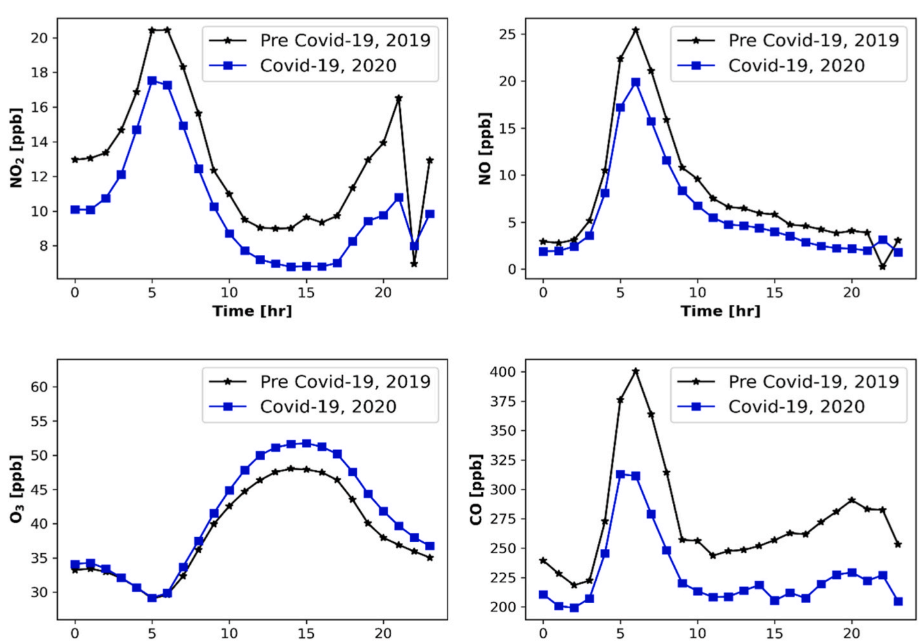


**Fig. 7.** Averaged diurnal cycles for the period of April to May for Covid-19 and pre- Covid-19 of a) $NO_2$, b) NO, c) $O_3$ and d) CO from ground-based measurements in Denver.

Reductions in NO lead to less $O_3$ degradation (through $NO + O_3 \rightarrow NO_2 + O_2$) under NOx saturated conditions, causing $O_3$ to increase by 4.7 ppb at mid-day (see Fig. S19). The increase in $O_3$ concentration during the conditions of reduced NOx concentrations is also known as the "weekend effect". Under high NOx conditions, less $NO_2$ leads to less consumption of OH in the $NO_2$ + OH reaction, increasing OH. To quantify the expected change in OH concentration due to the decrease in NOx and CO emission, the CLASS box model is used (described in section 3.5).

Yearly variations in emission and meteorological conditions influence $O_3$ in the urban plume. To account for this variability, five-year averaged ground-based measurement data (2015–2019) are used to derive a reference climatology for comparison to 2020 (Fig. S21). The comparison of five year averaged data (2015–2019) with 2020 shows that NO, $NO_2$, and CO decrease by 71.4%, 52.1%, and 30% respectively whereas $O_3$ increases by 1.5 ppb. The year 2017 had extremely high ozone concentrations in April compared to 2020 and resulted in a small decrease in $O_3$ concentration. However, in May 2020 $O_3$ concentrations are higher by 3.5 ppb in the afternoon compared to the five-year averaged data (Fig. S22).

### 3.5. CLASS vs ground-based measurements

To test if the CLASS model can reproduce the observed changes in Denver during 2020, modelled diurnal cycles of NO, $NO_2$, $O_3$, and CO are compared to measurements from three ground based stations i.e. Denver 1, Denver 2, and Adams that measure NO, $NO_2$,$O_3$ and CO simultaneously, averaged over April to May in 2019 and 2020. The CLASS model is run to simulate the spatially average NO, $NO_2$, $O_3$, and CO concentrations over Denver during 8h (8 a.m.–16 p.m.) for pre-Covid-19 and Covid-19 (see Tables S5 and S6 for details of the CLASS setup that has been used).

CLASS can reproduce the morning rush hour peak in NO, $NO_2$, and CO, and subsequent reductions during the afternoon (see Fig. 8) with a mean absolute error of −0.73 ppb, 0.44 ppb and 0.04 ppb respectively. CLASS captures the increase of $O_3$ concentration, reaching maximum in the afternoon due to photochemical production (see Fig. 8). To simulate the average NO, $NO_2$, and $O_3$ concentrations during Covid-19, the NOx and CO emissions are reduced by 70% and 40%, respectively, compared with pre-Covid-19 (see Table S5). CLASS is able to reproduce the observed reduction in NO, $NO_2$, and CO concentrations and increase in $O_3$ (see Fig. 8) during the Covid-19 lockdown. As expected from the diurnal cycle in solar insolation, the CLASS simulated diurnal cycle of OH reaches a maximum in the early afternoon (see Fig. 9). Reductions in $NO_x$ and CO emissions during Covid-19 increase OH by 51.3% during the mid-day (12 LST to 14 LST). This OH change in CLASS compares well to TROPOMI (28 ± 9%). A sensitivity test in which emissions of isoprene are increased by a factor of 1.5 along with $NO_x$ and CO emission reductions also shows an increase in midday OH by 62.4% (see Fig. S23).

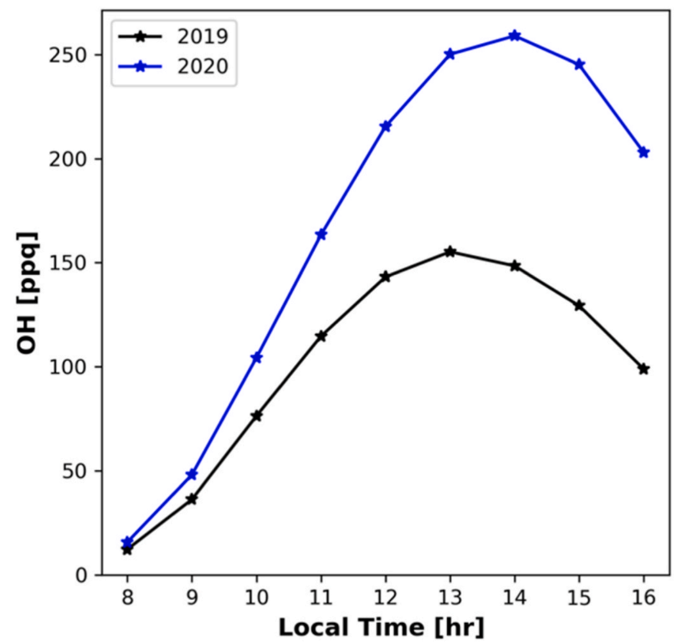


**Fig. 9.** CLASS simulated OH for 2019 and 2020 over Denver.

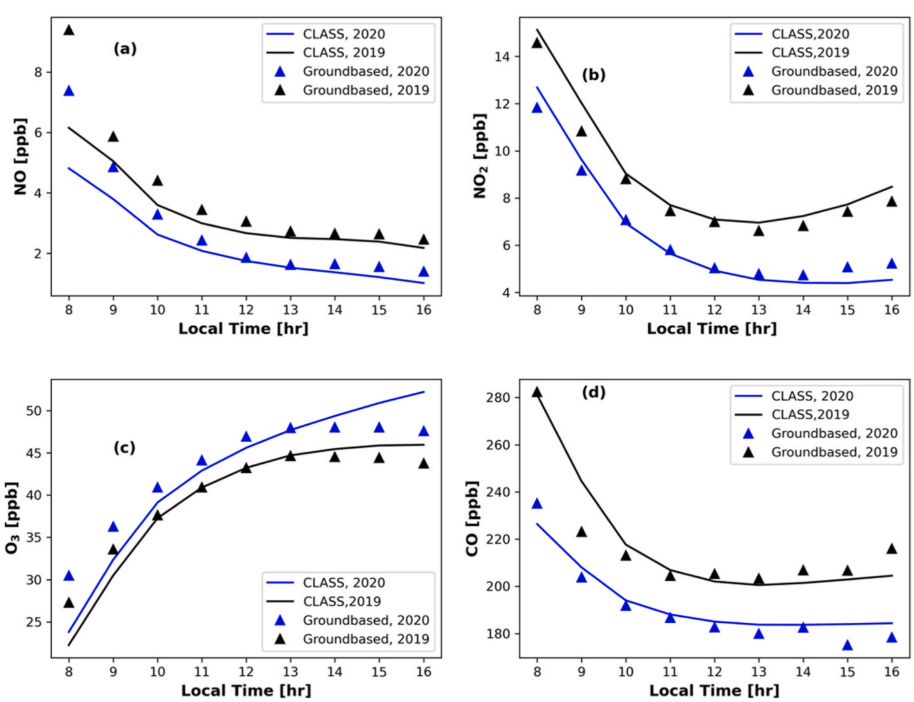


**Fig. 8.** The mean mixing ratio of a) NO, b) $NO_2$, c) $O_3$ and d) CO in Denver simulated by the CLASS model (solid line) and observed by the surface network (triangles) using measurement stations Denver 1, Denver 2, and Adams averaged from April to May in 2019 and 2020.

Another sensitivity test is performed to isolate the impact of the NOx emission reduction on OH production. This test indicates that reduction in NOx emission contributes to 95.3% of the OH increase.

## 4. Discussion

From TROPOMI retrieved $NO_2$/CO ratios we infer a substantial reduction in $\tau_{NOx}$ over and directly downwind of large cities during Covid-19 lockdowns. For Denver, the satellite observations, ground-based observation, and the CLASS model agree on a $\tau_{NOx}$ decrease by 28 ± 9%. Sensitivity tests in the CLASS model indicate that the decrease in $\tau_{NOx}$ is driven by reduced NOx emission, which eventually increase OH concentration in urban plume because less OH is consumed by the $NO_2$ + OH reaction, and more OH is recycled. OH, is the main factor determining the lifetime of $NO_x$ during noon, this explains the reduction in $\tau_{NOx}$. The same mechanism can explain the decreases in $\tau_{NOx}$ inferred for other cities using TROPOMI data. A recent global study by Miyazaki et al. (2021) on urban photochemistry demonstrated that the free troposphere has become less oxidative in response to reductions in NOx emissions resulting in an increase of the $CH_4$ lifetime. In the NOx limited free troposphere, a NOx decrease is indeed expected to reduce OH, contrasting with the NOx rich urban conditions of our study.

Meteorological conditions such as temperature, radiation, and wind speed also influence the urban photochemistry, and therefore could also explain spatial and temporal variations in $\tau_{NOx}$ (Lang et al., 2015; Romer et al., 2018). Under clear sky conditions, $\tau_{NOx}$ is systematically lower due to the higher photolysis rates. Because of this, the selection of satellite data for clear sky conditions introduces a sampling bias. However, this bias is present both in the pre- Covid-19 and Covid-19 time windows and the sampling bias is therefore unlikely to explain differences between the two periods, unless cloud cover was significantly different. Differences in meteorology between pre- Covid-19 and Covid-19 can certainly contribute to the differences in $\tau_{NOx}$. However, meteorology is unlikely to have influenced $\tau_{NOx}$ in the same way across all the six megacities, increasing the likelihood that the $\tau_{NOx}$ changes are primarily caused by changes in $NO_x$ emissions. In city centres with strong emissions from traffic, the photochemical regime is known to be $NO_x$ saturated. Under these conditions, the oxidative capacity is limited by the removal of OH in reaction with $NO_2$, and decreasing $NO_x$ emission increase OH. Improvements in visibility due to reduced emissions and secondary formation of aerosols could also have contributed to $\tau_{NOx}$ decreases during Covid-19. However, our CLASS computations, which do not simulate changes in aerosol loading, indicate that reduced emissions of reactive trace gases are sufficient to explain the observed $\tau_{NOx}$ changes.

Further downwind of the city, the chemical conditions become favourable for OH formation and recycling, reducing $\tau_{NOx}$ (Romer Present et al., 2019; Sobanski et al., 2017; Valin et al., 2013). The exponential fit to the TROPOMI derived $NO_2$/CO ratio in the downwind urban plume provides an average estimate of $\tau_{NOx}$ and cannot distinguish between $\tau_{NOx}$ in the centre of city and its outskirts, despite our attempts to resolve this difference (not shown). However, future satellite instruments observing at higher temporal and spatial resolutions could provide more independent points over city, so the gradient in $NO_2$/CO ratio can be captured better. This can provide the information needed to study chemical processing in city plumes.

We do not have emission inventory estimates for 2020 but assume that traffic emissions reduced the most. Therefore, a sensitivity test has been performed for Denver in which traffic NOx and CO emissions are reduced by 45%, while keeping the other emissions sectors unchanged. According to EDGAR, this traffic emission reduction would increase the $NO_2$/CO ratio of the emissions by 28.5%. However, TROPOMI shows stronger reductions in NOx compared to CO resulting in a decrease in the $NO_2$/CO ratio close to centre of city during Covid-19 lockdown in all the cities we analyzed. Increases in OH due to reductions in NOx emissions under VOC limited photochemical conditions in city centres could partially explain the difference between TROPOMI and EDGAR derived $NO_2$/CO ratio changes. This provides another line of evidence that $NO_x$ lifetimes reduced during Covid-19 lockdowns. Besides traffic emissions, some industrial emission sectors likely also reduced during lockdowns, which could explain another part of the mismatch between TROPOMI and inventory data.

We verified the consistency of the observed $NO_2$ decrease and estimated OH increase with the EDGAR emission inventory. During the lockdown in Wuhan, EDGAR shows negligible emissions from aviation and road transport, and 80% reduction in the manufacturing industries. The combined impact is a reduction of the total $NO_x$ emission by 50%. TROPOMI shows stronger reduction in $NO_2$ of 65–80%, which is consistent with the simultaneous increase in OH that we derive.

This study shows that the reduction in emissions results in an increase in the urban atmospheric oxidative capacity, primarily driven by the presence of hydroxyl radicals (OH). This increased oxidative capacity enhances the degradation of reactive species through oxidation processes, ultimately contributing to improved air quality. However, it is important to note that the increased oxidative capacity can also promote additional photochemical reactions, leading to the formation of ozone ($O_3$) and secondary aerosols. Elevated levels of $O_3$ can have adverse effects on human health and ecosystems. Thus, while emission reductions have positive implications for air quality through enhanced oxidative degradation, careful consideration is necessary to mitigate the potential negative impacts of increased photochemical reactions and the subsequent formation of $O_3$ and secondary aerosols. This study shows that $NO_2$/CO ratio from satellite observations can be used to test how well photochemistry models are capable of simulating the dynamics in urban OH.

In this study, strong isolated sources of $NO_2$ and CO have been selected to estimate the NOx lifetime. In regions with more complex emission distributions, calm conditions can be selected to derive $\tau_{NOx}$ when the $NO_2$ and CO plumes are concentrated close to the source. In addition, our method needs $NO_x$ and CO emissions that are large enough to be readily detectable from space. In European cities, CO emission have been reduced in the past to levels that are barely detectable by TROPOMI. In such cases our method cannot be used.

## 5. Conclusion

In this study, TROPOMI derived $XNO_2$, XCO, and $XNO_2$/XCO ratios are used to study changes in the urban photochemistry during Covid-19 lockdowns. An exponential function fitted method is used to estimate the chemical lifetime of $NO_x$ from TROPOMI retrieved $NO_2$/CO ratios in the downwind urban plume of large megacities. $\tau_{NOx}$ has been estimated for six different megacities (Riyadh, Wuhan, Sao- Paulo, Chicago, Denver, and New York) during Covid-19 and the year before, to analyse the impact of Covid-19 lockdowns on urban photochemistry. To account for influences of wind speed, $\tau_{NOx}$ is determined for calm and windy day separately. For windy days, $\tau_{NOx}$ has been derived for Riyadh, Chicago and New York only, because the data availability was insufficient for the other cities.

The Covid-19 lockdown reduced urban $NO_2$ concentrations by 30–50% in the cities of Riyadh, Denver, Chicago, Sao-Paulo, and New York. Wuhan adopted a stricter lockdown policy compared to the other megacities leading to a larger reduction in $NO_2$ concentration (65–80%). Close to centre of city, XCO showed smaller reductions (10–15%) over Wuhan and New York. In contrast, the XCO background concentration increased during Covid-19 in Riyadh, Denver, Chicago, and Sao-Paulo by 5–10%.

Except over Riyadh during windy days, our results show a systematic reduction in $\tau_{NOx}$ during Covid-19 lockdowns. For the calm days, a large difference in $\tau_{NOx}$ is observed over Sao-Paulo (31.8 ± 9.0%), whereas a relatively small change in $\tau_{NOx}$ is found for Riyadh (22 ± 6.6%). Similarly, windy days over New York and Chicago also show shorter $\tau_{NOx}$ during the Covid-19 lockdown than pre- Covid-19. Only in the case of windy days over Riyadh a similar $\tau_{NOx}$ is observed during Covid-19 and pre-covid-19.

The ground-based measurement and the CLASS model have been used to study the impact of the covid lockdown on the urban photochemistry in Denver, confirming the satellite derived $\tau_{NOx}$ reductions. The CLASS model reproduced the observed increase in $O_3$ concentration by 4.0 ppb in response to the observed reductions in NO (38.7%) and $NO_2$ (25.7%) concentration during covid. The decreased NOx emission results in a reduced consumption of OH in the $NO_2$ + OH reaction, eventually increasing OH in the urban plume which is displayed by CLASS and indicating the reason for shorter $\tau_{NOx}$ during Covid-19 lockdown at mid-day. The relative change in $\tau_{NOx}$ estimated by TROPOMI (28 ± 9%) is consistent with the CLASS simulations, initialized using the ground-based measurements in Denver.

This study demonstrates how satellite measurements of $NO_2$ and CO can be used to study urban photochemistry in polluted cities around the world, providing a new observation-based method to evaluate the models that are used for monitoring urban air quality. The changes that are detected during Covid-19 lockdowns provide an observational based quantification of air quality benefits that are to be expected from the energy transition, which can be monitored from space using the method presented in this study.

## CRediT authorship contribution statement

**Srijana Lama:** Formal analysis, performed the data analysis and data interpretation and wrote the paper, discussed the results. **Sander Houweling:** Supervision, supervised the study, discussed the results. **K. Folkert Boersma:** discussed the results. **Ilse Aben:** discussed the results. **Hugo A.C. Denier van der Gon:** discussed the results, All co-authors commented on the paper and improved it. **Maarten C. Krol:** discussed the results.

## Declaration of competing interest

The authors declare that they have no conflict of interest.

## Data availability

I have shared the data link in the manuscript.

## Acknowledgements

This research has been supported by the Aard- en Levenswetenschappen, Nederlandse Organisatie voor Wetenschappelijk Onderzoek (grant no. 2017.036). Thanks to prof Dr. Jordi Vila-Guerau de Arellano for providing the guidance to setup CLASS model.

## Appendix A. Supplementary data

Supplementary data to this article can be found online at https://doi.org/10.1016/j.atmosenv.2023.120042.

## References


Beirle, S., Boersma, K.F., Platt, U., Lawrence, M.G., Wagner, T., 2011. Megacity emissions and lifetimes of nitrogen oxides probed from space. Science 84 333, 1737–1739. https://doi.org/10.1126/science.1207824.

Beirle, S., Borger, C., Dörner, S., Li, A., Hu, Z., Liu, F., Wang, Y., Wagner, T., 2019. Pinpointing nitrogen oxide emissions from space. Sci. Adv. 5, 1–7. https://doi.org/10.1126/sciadv.aax9800.

Boersma, K.F., Eskes, H.J., Dirksen, R.J., Van Der A, R.J., Veefkind, J.P., Stammes, P., Huijnen, V., Kleipool, Q.L., Sneep, M., Claas, J., Leitão, J., Richter, A., Zhou, Y., Brunner, D., 2011. An improved tropospheric NO2 column retrieval algorithm for the Ozone Monitoring Instrument. Atmos. Meas. Tech. 4, 1905–1928. https://doi.org/10.5194/amt-4-1905-2011.

Boersma, K.F., Eskes, H.J., Richter, A., De Smedt, I., Lorente, A., Beirle, S., Van Geffen, J. H.G.M., Zara, M., Peters, E., Van Roozendael, M., Wagner, T., Maasakkers, J.D., Van Der A, R.J., Nightingale, J., De Rudder, A., Irie, H., Pinardi, G., Lambert, J.C., Compernolle, S.C., 2018. Improving algorithms and uncertainty estimates for satellite NO2 retrievals: results from the quality assurance for the essential climate variables (QA4ECV) project. Atmos. Meas. Tech. 11, 6651–6678. https://doi.org/10.5194/amt-11-6651-2018.

Bonaccorsi, G., Pierri, F., Cinelli, M., Flori, A., Galeazzi, A., Porcelli, F., Schmidt, A.L., Valensise, C.M., Scala, A., Quattrociocchi, W., Pammolli, F., 2020. Economic and social consequences of human mobility restrictions under COVID-19. Proc. Natl. Acad. Sci. U.S.A. 117, 15530–15535. https://doi.org/10.1073/pnas.2007658117.

Borsdorff, T., Aan de Brugh, J., Hu, H., Aben, I., Hasekamp, O., Landgraf, J., 2018b. Measuring carbon monoxide with TROPOMI: first results and a comparison with ECMWF-IFS analysis data. Geophys. Res. Lett. 45, 2826–2832. https://doi.org/10.1002/2018GL077045.

Borsdorff, T., Aan De Brugh, J., Pandey, S., Hasekamp, O., Aben, I., Houweling, S., Landgraf, J., 2019. Carbon monoxide air pollution on sub-city scales and along arterial roads detected by the Tropospheric Monitoring Instrument. Atmos. Chem. Phys. 19, 3579–3588. https://doi.org/10.5194/acp-19-3579-2019.

Borsdorff, Tobias, Andrasec, J., De Brugh, J.A., Hu, H., Aben, I., Landgraf, J., 2018a. Detection of carbon monoxide pollution from cities and wildfires on regional and urban scales: the benefit of CO column retrievals from SCIAMACHY 2.3 µm measurements under cloudy conditions. Atmos. Meas. Tech. 11, 2553–2565. https://doi.org/10.5194/amt-11-2553-2018.

Borsdorff, T., de Brugh, J., Hu, H., Hasekamp, O., Sussmann, R., Rettinger, M., Hase, F., Gross, J., Schneider, M., Garcia, O., Stremme, W., Grutter, M., Feist, D.G., Arnold, S. G., De Mazière, M., Kumar Sha, M., Pollard, D.F., Kiel, M., Roehl, C., Wennberg, P.O., Toon, G.C., Landgraf, J., 2018c. Mapping carbon monoxide pollution from space down to city scales with daily global coverage. Atmos. Meas. Tech. 11, 5507–5518. https://doi.org/10.5194/amt-11-5507-2018.

Borsdorff, T., Hasekamp, O.P., Wassmann, A., Landgraf, J., 2014. Insights into Tikhonov regularization: application to trace gas column retrieval and the efficient calculation of total column averaging kernels. Atmos. Meas. Tech. 7, 523–535. https://doi.org/10.5194/amt-7-523-2014.

Bray, C.D., Nahas, A., Battye, W.H., Aneja, V.P., 2020. Impact of lockdown during the COVID-19 outbreak on multi-scale air quality. Atmos. Environ. 254, 118386 https://doi.org/10.1016/j.atmosenv.2021.118386.

Chauhan, A., Singh, R.P., 2020. Decline in PM2.5 concentrations over major cities around the world associated with COVID-19. Environ. Res. 187, 109634 https://doi.org/10.1016/j.envres.2020.109634.

Dekker, I.N., Houweling, S., Aben, I., Röckmann, T., Krol, M., Martínez-Alonso, S., Deeter, M.N., Worden, H.M., 2017. Quantification of CO emissions from the city of madrid using MOPITT satellite retrievals and WRF simulations. Atmos. Chem. Phys. 17, 14675–14694. https://doi.org/10.5194/acp-17-14675-2017.

Dekker, I.N., Houweling, S., Pandey, S., Krol, M., Röckmann, T., Borsdorff, T., Landgraf, J., Aben, I., 2019. What caused the extreme CO concentrations during the 2017 high-pollution episode in India? Atmos. Chem. Phys. 19, 3433–3445. https://doi.org/10.5194/acp-19-3433-2019.

Dhaka, S.K., Chetna Kumar, V., Panwar, V., Dimri, A.P., Singh, N., Patra, P.K., Matsumi, Y., Takigawa, M., Nakayama, T., Yamaji, K., Kajino, M., Misra, P., Hayashida, S., 2020. PM2.5 diminution and haze events over Delhi during the COVID-19 lockdown period: an interplay between the baseline pollution and meteorology. Sci. Rep. 10, 1–8. https://doi.org/10.1038/s41598-020-70179-8.

Eskes, H.J., Eichmann, K.U., 2022. S5P mission performance centre nitrogen dioxide [L2 _NO2_ _] readme document. S5P-MPC-KNMI-PRF-NO2, KNMI. available at: https://sentinel.esa.int/documents/247904/3541451/Sentinel-5P-Nitrogen-Dioxide-Level-2-Product-Readme-File. .

Eskes, H.J., van Geffen, J., Boersma, K.F., Eichmann, K.-U., Apituley, A., Pedergnana, M., Sneep, M., Pepijn, J., Loyola, D., 2018. Level 2 Product User Manual Henk Eskes, S5P-KNMI-L2-0021-MA, issue 3.0.0. https://earth.esa.int/documents/247904/2474726/Sentinel-5P-Level-2-Product-User-Manual-Nitrogen-Dioxide (last access: 27 March 2019).

Filonchyk, M., Hurynovich, V., Yan, H., Gusev, A., Shpilevskaya, N., 2020. Impact assessment of covid-19 on variations of so2, no2, co and aod over east China. Aerosol Air Qual. Res. 20, 1530–1540. https://doi.org/10.4209/aaqr.2020.05.0226.

Goldberg, D.L., Anenberg, S.C., Griffin, D., McLinden, C.A., Lu, Z., Streets, D.G., 2020. Disentangling the impact of the COVID-19 lockdowns on urban NO2 from natural variability. Geophys. Res. Lett. 47 https://doi.org/10.1029/2020GL089269.

Gong, D.Y., Wang, W., Qian, Y., Bai, W., Guo, Y., Mao, R., 2014. Observed holiday aerosol reduction and temperature cooling over East Asia. J. Geophys. Res. 119, 6306–6324. https://doi.org/10.1002/2014JD021464.

Huijnen, V., Pozzer, A., Arteta, J., Brasseur, G., Bouarar, I., Chabrillat, S., Christophe, Y., Doumbia, T., Flemming, J., Guth, J., Josse, B., Karydis, V.A., Marécal, V., Pelletier, S., 2019. Quantifying uncertainties due to chemistry modelling - evaluation of tropospheric composition simulations in the CAMS model (cycle 43R1). Geosci. Model Dev. (GMD) 12, 1725–1752. https://doi.org/10.5194/gmd-12-1725-2019.

Krol, M., Houweling, S., Bregman, B., Broek, M. Van Den, Segers, A., Velthoven, P. Van, Peters, W., Dentener, F., 2005. The two-way nested global chemistry-transport zoom model TM5 : algorithm and applications. Atmos. Chem. Phys. 417–432. https://doi.org/10.5194/acp-5-417-2005.

Lama, S., Houweling, S., Boersma, K.F., Aben, I., van der Gon, H.A.C.D., Krol, M.C., 2022. Estimation of OH in urban plume using TROPOMI inferred $NO_2$/CO. Atmos. Chem. Phys. 22, 16053–16071. https://doi.org/10.5194/acp-22-16053-2022.

Lama, S., Houweling, S., Folkert Boersma, K., Eskes, H., Aben, I., Denier Van Der Gon, A. C., Krol M, H.C., Dolman, H., Borsdorff, T., Lorente, A., 2020. Quantifying burning efficiency in megacities using the $NO_2$/CO ratio from the Tropospheric Monitoring Instrument (TROPOMI). Atmos. Chem. Phys. 20, 10295–10310. https://doi.org/10.5194/acp-20-10295-2020.

Lambert, J.-C., Keppens, A., Hubert, D., Langerock, B., E, K.U., Kleipool, Q., Sneep, M., Verhoelst, T., Wagner, T., Weber, M., Ahn, C., Balis, A.A.D., Chan, K.L., Compernolle, S., De Smedt, I., Eskes, H., Garane, A.M.F.K., Gleason, J.F., Goutail, F., Granville, J., Hedelt, P., Jaross, K.-P.H.G., Koukouli, M.L., Landgraf, J., Lutz, R., Niemejer, S., Pinardi, A.P.G., Pommereau, J.-P., Richter, A., Rozemeijer, N., Sha, M. K., Zweers, D.S., Theys, N., Tilstra, G., Torres, O., Valks, P., Vigouroux, C., P.W., 2019. Sentinel-5 Precursor Mission Performance Centre Quarterly Validation Report of the Copernicus Sentinel-5 Precursor Operational Data Products # 03. July 2018 – May 2019 1–125.

Landgraf, J., de Brugh, J., Scheepmaker, R., Borsdorff, T., Hu, H., Houweling, S., Butz, A., Aben, I., Hasekamp, O., 2016. Carbon monoxide total column retrievals from TROPOMI shortwave infrared measurements. Atmos. Meas. Tech. 9, 4955–4975. https://doi.org/10.5194/amt-9-4955-2016.

Lang, M.N., Gohm, A., Wagner, J.S., 2015. The impact of embedded valleys on daytime pollution transport over a mountain range. Atmos. Chem. Phys. https://doi.org/10.5194/acp-15-11981-2015.

Lange, K., Richter, A., Burrows, J.P., 2021. Variability of nitrogen oxide emission fluxes and lifetimes estimated from Sentinel-5P TROPOMI observations. Atmos. Chem. Phys. Discuss. 2, 1–32. https://doi.org/10.5194/acp-2021-273.

Laughner, J., Cohen, R.C., 2019. Direct observation of changing NOx lifetime in NOrth American cities. Science 84 366, 723–727. https://doi.org/10.1126/science.aax6832.

Le, T., Wang, Y., Liu, L., Yang, J., Yung, Y.L., Li, G., Seinfeld, J.H., 2020. Unexpected air pollution with marked emission reductions during the COVID-19 outbreak in China. Science 84 369, 702–706. https://doi.org/10.1126/science.abb7431.

Liu, F., Beirle, S., Zhang, Q., Dörner, S., He, K., Wagner, T., 2016. NOx lifetimes and emissions of cities and power plants in polluted background estimated by satellite observations. Atmos. Chem. Phys. 16, 5283–5298. https://doi.org/10.5194/acp-16-5283-2016.

Liu, F., Beirle, S., Zhang, Q., Van Der A, R.J., Zheng, B., Tong, D., He, K., 2017. NOx emission trends over Chinese cities estimated from OMI observations during 2005 to 2015. Atmos. Chem. Phys. https://doi.org/10.5194/acp-17-9261-2017.

Lorente, A., Boersma, K.F., Eskes, H.J., Veefkind, J.P., van Geffen, J.H.G.M., de Zeeuw, M.B., Denier van der Gon, H.A.C., Beirle, S., Krol, M.C., 2019. Quantification of nitrogen oxides emissions from build-up of pollution over Paris with TROPOMI. Sci. Rep. 9, 1–10. https://doi.org/10.1038/s41598-019-56428-5.

Lorente, A., Folkert Boersma, K., Yu, H., Dörner, S., Hilboll, A., Richter, A., Liu, M., Lamsal, L.N., Barkley, M., De Smedt, I., Van Roozendael, M., Wang, Y., Wagner, T., Beirle, S., Lin, J.T., Krotkov, N., Stammes, P., Wang, P., Eskes, H.J., Krol, M., 2017. Structural uncertainty in air mass factor calculation for NO2 and HCHO satellite retrievals. Atmos. Meas. Tech. 10, 759–782. https://doi.org/10.5194/amt-10-759-2017.

McKibbin, W., Fernando, R., 2021. The global macroeconomic impacts of COVID-19: seven scenarios. Asian Econ. Pap. 20, 1–30. https://doi.org/10.1162/asep_a_00796.

Misra, P., Takigawa, M., Khatri, P., Dhaka, S.K., Dimri, A.P., Yamaji, K., Kajino, M., Takeuchi, W., Imasu, R., Nitta, K., Patra, P.K., Hayashida, S., 2021. Nitrogen oxides concentration and emission change detection during COVID-19 restrictions in North India. Sci. Rep. 11, 1–11. https://doi.org/10.1038/s41598-021-87673-2.

Miyazaki, K., Bowman, K., Sekiya, T., Takigawa, M., Neu, J.L., Sudo, K., Osterman, G., Eskes, H., 2021. Global tropospheric ozone responses to reduced NOx emissions linked to the COVID-19 worldwide lockdowns. Sci. Adv. 7, 1–15. https://doi.org/10.1126/sciadv.abf7460.

Ouwersloot, H. G., Vilà-Guerau de Arellano, J., Nölscher, A. C., Krol, M. C., Ganzeveld, L. N., Breitenberger, C., Mammarella, I., Williams, J., Lelieveld, J., 2012. Characterization of a boreal convective boundary layer and its impact on atmospheric chemistry during HUMPPA-COPEC-2010. Atmos. Chem. Phys. 12, 9335–9353. https://doi.org/10.5194/acp-12-9335-2012.

Pommier, M., McLinden, C.A., Deeter, M., 2013. Relative changes in CO emissions over megacities based on observations from space. Geophys. Res. Lett. 40, 3766–3771. https://doi.org/10.1002/grl.50704.

Riess, T.C.V.W., Boersma, K.F., Van Vliet, J., Peters, W., Sneep, M., Eskes, H., Van Geffen, J., 2022. Improved monitoring of shipping NO2 with TROPOMI: decreasing NOx emissions in European seas during the COVID-19 pandemic. Atmos. Meas. Tech. 15, 1415–1438. https://doi.org/10.5194/amt-15-1415-2022.

Romano, S., Catanzaro, V., Paladini, F., 2021. Impacts of the covid-19 lockdown measures on the 2020 columnar and surface air pollution parameters over south-eastern Italy. Atmosphere. https://doi.org/10.3390/atmos12101366.

Romer, P.S., Duffey, K.C., Wooldridge, P.J., Edgerton, E., Baumann, K., Feiner, P.A., Miller, D.O., Brune, W.H., Koss, A.R., De Gouw, J.A., Misztal, P.K., Goldstein, A.H., Cohen, R.C., 2018. Effects of temperature-dependent NOx emissions on continental ozone production. Atmos. Chem. Phys. https://doi.org/10.5194/acp-18-2601-2018.

Romer Present, P.S., Zare, A., Cohen, R.C., 2019. The changing role of organic nitrates in the removal and transport of NOx. Atmos. Chem. Phys. Discuss. 1–18. https://doi.org/10.5194/acp-2019-471.

Sha, M.K., Langerock, B., Blavier, J.-F.L., Blumenstock, T., Borsdorff, T., Buschmann, M., Dehn, A., De Mazière, M., Deutscher, N.M., Feist, D.G., García, O.E., Griffith, D.W.T., Grutter, M., Hannigan, J.W., Hase, F., Heikkinen, P., Hermans, C., Iraci, L.T., Jeseck, P., Jones, N., Kivi, R., Kumps, N., Landgraf, J., Lorente, A., Mahieu, E., Makarova, M.V., Mellqvist, J., Metzger, J.-M., Morino, I., Nagahama, T., Notholt, J., Ohyama, H., Ortega, I., Palm, M., Petri, C., Pollard, D.F., Rettinger, M., Robinson, J., Roche, S., Roehl, C.M., Röhling, A.N., Rousogenous, C., Schneider, M., Shiomi, K., Smale, D., Stremme, W., Strong, K., Sussmann, R., Té, Y., Uchino, O., Velazco, V.A., Vigouroux, C., Vrekoussis, M., Wang, P., Warneke, T., Wizenberg, T., Wunch, D., Yamanouchi, S., Yang, Y., Zhou, M., 2021. Validation of methane and carbon monoxide from Sentinel-5 Precursor using TCCON and NDACC-IRWG stations. Atmos. Meas. Tech. 14, 6249–6304. https://doi.org/10.5194/amt-14-6249-2021.

Sobanski, N., Thieser, J., Schuladen, J., Sauvage, C., Song, W., Williams, J., Lelieveld, J., Crowley, J.N., 2017. Day and night-time formation of organic nitrates at a forested mountain site in south-west Germany. Atmos. Chem. Phys. https://doi.org/10.5194/acp-17-4115-2017.

Valin, L.C., Russell, A.R., Cohen, R.C., 2013. Variations of OH radical in an urban plume inferred from NO 2 column measurements. Geophys. Res. Lett. https://doi.org/10.1002/grl.50267.

Valin, L.C., Russell, A.R., Hudman, R.C., Cohen, R.C., 2011. Effects of model resolution on the interpretation of satellite NO2 observations. Atmos. Chem. Phys. 11, 11647–11655. https://doi.org/10.5194/acp-11-11647-2011.

Van Geffen, J., Eskes, H., Compernolle, S., Pinardi, G., Verhoelst, T., Lambert, J.C., Sneep, M., Linden, M. Ter, Ludewig, A., Folkert Boersma, K., Pepijn Veefkind, J., 2022. Sentinel-5P TROPOMI NO2retrieval: impact of version v2.2 improvements and comparisons with OMI and ground-based data. Atmos. Meas. Tech. 15, 2037–2060. https://doi.org/10.5194/amt-15-2037-2022.

van Geffen, J.H.G.M., Eskes, H.J., Boersma, K.F., Maasakkers, J.D., Veefkind, J.P., 2019. TROPOMI ATBD of the Total and Tropospheric NO2 Data Products, S5P-KNMI-L2-0005-RP, Issue 1.4.0, 6 Feburary 2019. S5P-Knmi-L2-0005-Rpp. 1–76.

Van Stratum, B.J.H., Vilá-Guerau De Arellano, J., Ouwersloot, H.G., Van Den Dries, K., Van Laar, T.W., Martinez, M., Lelieveld, J., Diesch, J.M., Drewnick, F., Fischer, H., Hosaynali Beygi, Z., Harder, H., Regelin, E., Sinha, V., Adame, J.A., Sörgel, M., Sander, R., Bozem, H., Song, W., Williams, J., Yassaa, N., 2012. Case study of the diurnal variability of chemically active species with respect to boundary layer dynamics during DOMINO. Atmos. Chem. Phys. 12, 5329–5341. https://doi.org/10.5194/acp-12-5329-2012.

Veefkind, J.P., Aben, I., McMullan, K., Förster, H., de Vries, J., Otter, G., Claas, J., Eskes, H.J., de Haan, J.F., Kleipool, Q., van Weele, M., Hasekamp, O., Hoogeveen, R., Landgraf, J., Snel, R., Tol, P., Ingmann, P., Voors, R., Kruizinga, B., Vink, R., Visser, H., Levelt, P.F., 2012. TROPOMI on the ESA Sentinel-5 Precursor: a GMES mission for global observations of the atmospheric composition for climate, air quality and ozone layer applications. Remote Sens. Environ. https://doi.org/10.1016/j.rse.2011.09.027.

Vila-Guerau de Arellano, K., Pino, D., 2009. On inferring isoprene emission surface flux from atmospheric boundary layer concentration measurements. Atmos. Chem. Phys. 9, 3629–3640. https://doi.org/10.5194/acp-9-3629-2009.

Vinken, G.C.M., Boersma, K.F., Jacob, D.J., Meijer, E.W., 2011. Accounting for non-linear chemistry of ship plumes in the GEOS-Chem global chemistry transport model. Atmos. Chem. Phys. 11, 11707–11722. https://doi.org/10.5194/acp-11-11707-2011.

Vîrghileanu, Mihai, Nistor, C., Vîrghileanu, B., 2020. Nitrogen Dioxide (NO2) Pollution monitoring with Sentinel-5P satellite imagery over Europe during the coronavirus pandemic outbreak. Rem. Sens. 12 (21), 3575. https://doi.org/10.3390/rs12213575.

Xu, K., Cui, K., Young, L.H., Hsieh, Y.K., Wang, Y.F., Zhang, J., Wan, S., 2020. Impact of the COVID-19 event on air quality in central China. Aerosol Air Qual. Res. 20, 915–929. https://doi.org/10.4209/aaqr.2020.04.0150.

Zara, M., Boersma, K.F., Eskes, H., Denier van der Gon, H., Vilà-Guerau de Arellano, J., Krol, M., van der Swaluw, E., Schuch, W., Velders, G.J.M., 2021. Reductions in nitrogen oxides over The Netherlands between 2005 and 2018 observed from space and on the ground: decreasing emissions and increasing O3 indicate changing NOx chemistry. Atmos. Environ. X 9. https://doi.org/10.1016/j.aeaoa.2021.100104.

Zhang, Q., Boersma, K.F., Zhao, B., Eskes, H., Chen, C., Zheng, H., Zhang, X., 2023. Quantifying daily NOx and CO2 emissions from Wuhan using satellite observations from TROPOMI and OCO-2. Atmos. Chem. Phys. 23, 551–563. https://doi.org/10.5194/acp-23-551-2023.